

RESEARCH

Open Access



Antineoplastic activity of *Artemisia annua* bio-United Fe₃O₄/CeO₂ on 4T1 breast cancer cells: in vivo and in vitro

Ziba Ahmadi¹, Abolfazl Bayrami^{1*} , Saber Zahri¹, Shima Rahim Pouran^{2*} and Aziz Habibi-Yangjeh³

*Correspondence:

abolfalbayrami@gmail.com; a_bayrami@uma.ac.ir; rahimpooran@yahoo.com; rahimpooran@uma.ac.ir

¹ Department of Biology, Faculty of Science, University of Mohaghegh Ardabili, Ardabil, Iran

² Faculty of Agriculture and Natural Resources, University of Mohaghegh Ardabili, Ardabil, Iran

³ Department of Chemistry, Faculty of Science, University of Mohaghegh Ardabili, Ardabil, Iran

Abstract

Breast cancer has become the most prevalent malignancy among women, and it is estimated to comprise over 30% of all cancer cases diagnosed in women. This study evaluates the antitumor effects of a green-synthesized Fe₃O₄/CeO₂ nanocomposite, utilizing *Artemisia annua* L. extract, against breast cancer. The viability assay was carried out using 100 to 1000 µg/mL of the as-prepared nanocomposites. The BALB/c mice were injected with 4T1 breast cancer cells and subsequently treated with 5 mg/kg body weight of the synthesized nanocomposites through intraperitoneal injection for two weeks. The in vitro studies on the cell viability and cytotoxicity of Fe₃O₄/CeO₂ nanocomposites demonstrated superior effectiveness of the green-synthesized sample (AFC) compared to the chemically produced variant (FC) against 4T1 cells. Treatment with AFC significantly reduced tumor size in 4T1-injected BALB/c mice compared to untreated control. The IC50 results for FC (890.16 µg/mL) and AFC (490.21 µg/mL) corroborated these findings. Notably, the biointerface provided by the phytochemicals from *A. annua* extract played a crucial role in enhancing the cytotoxic effects of the nanocomposite. This research highlights the potential of green-synthesized Fe₃O₄/CeO₂ nanocomposites as a safe and effective nanomedicine for targeting cancer cells while minimizing adverse effects on healthy cells.

Keywords: *Artemisia annua* L., Breast cancer, 4T1 cell line, Fe₃O₄/CeO₂, Magnetic nanobiocomposite

Background

With a mortality rate of about ten million people per year, cancer and cancer-related diseases are among the leading causes of death all over the globe (Ferlay et al. 2020). Nevertheless, far too little information is available regarding the biology of metastasis (Riggio et al. 2021). Even though numerous antineoplastic agents with promising outcomes have been drafted over the last decades, many were abandoned pending clinical trials due to their potential toxicity and side effects (Dy and Adjei 2013). Cancer development is associated with several determinants, e.g., genetic, hormonal, lifestyle, cultural, social, and environmental factors (Manouchehri et al. 2022). According to the latest data in 2021, breast cancer has emerged as the most prevalent and widespread malignancy in women,



© The Author(s) 2024. **Open Access** This article is licensed under a Creative Commons Attribution-NonCommercial-NoDerivatives 4.0 International License, which permits any non-commercial use, sharing, distribution and reproduction in any medium or format, as long as you give appropriate credit to the original author(s) and the source, provide a link to the Creative Commons licence, and indicate if you modified the licensed material. You do not have permission under this licence to share adapted material derived from this article or parts of it. The images or other third party material in this article are included in the article's Creative Commons licence, unless indicated otherwise in a credit line to the material. If material is not included in the article's Creative Commons licence and your intended use is not permitted by statutory regulation or exceeds the permitted use, you will need to obtain permission directly from the copyright holder. To view a copy of this licence, visit <http://creativecommons.org/licenses/by-nc-nd/4.0/>.

and it is anticipated that it encloses over 30% of all cancer cases detected in women (Ferlay et al. 2020; Arnold et al. 2022). Presently, the conventional approaches to diagnose breast cancer involve procedures such as mammography, MRI scans, biopsies, and the examination of tumor tissue for traditional indicators such as estrogen and progesterone receptors (ER, PR), human epidermal growth factor type 2 receptor (HER2), proliferation index (Ki67), and cytokeratins (CK5/6, CK14, C19). In recent times, these diagnostic techniques have been enhanced by contemporary molecular methods, such as next-generation sequencing, in situ hybridization, and microRNA analysis, which serve to identify emerging molecular markers (Beňačka et al. 2022). The available breast cancer treatment options encompass traditional surgical procedures, chemotherapy, radiation therapy, hormonal therapy, as well as emerging medications designed to target specific biological markers and gene therapy (Waks and Winer 2019). Chemotherapy (CT) can be administered either before (known as neoadjuvant CT) or after (called adjuvant CT) the surgical procedure, during the maintenance phase, or even in a palliative setting for patients with metastatic tumors (Pellegrini et al. 2023). Although the therapies targeting the human epidermal growth factor receptor 2 (HER2), e.g., chemotherapy and radiation therapy, are effective in treating early-stage breast cancer, they are ineffective when dealing with advanced-stage cancers. This is because chemotherapy drugs generally fail to specifically target the cancer cells and unintentionally harm healthy cells (Davezac et al. 2023). Moreover, they can lead to significant harm to the central nervous system (known as chemobrain) and heart and blood vessels at high doses (Zajęczkowska et al. 2019). For instance, the conventional chemotherapeutic agents used in cancer treatment such as mitoxantrone (MTX) and doxorubicin (DOX) can also cause heart-related side effects (Brandão et al. 2023). Additionally, patients undergoing chemotherapy are more susceptible to infections, which can lead to complications including colitis, mucositis, sepsis, and diarrhoea (Singh et al. 2023). On the other hand, the minimally invasive therapies, including laser ablation, cryotherapy, and radiofrequency ablation (RFA), are also introduced for early-stage breast cancer treatment. Currently, the most frequently employed therapies for breast cancer typically involve the combination of two drug treatments, such as doxorubicin (Adriamycin), docetaxel (Taxotere), and cyclophosphamide (TAC) (Brown et al. 2021).

In the realm of cancer research, one widely explored avenue is nanotechnology. Nanotechnology has yielded several nanomaterials with promising outcomes in their applications for cancer, encompassing cancer diagnosis, drug transport and delivery, targeted therapy, gene therapy, molecular imaging, and biomarker mapping. Nanotechnology not only allows for the precise targeting of neoplasms and cancerous cells, but also facilitates the detection of tumor sites and enhances the effectiveness of traditional treatment methods (Jin et al. 2020; Wang et al. 2023). Over the recent years, nanoparticles have been extensively studied for their role as carriers in drug delivery for cancer diagnosis and treatment. They have the potential to enhance the biological availability and effectiveness of barely soluble and unstable medications with prolonged circulation in the bloodstream, reduce overall toxicity, increase cellular uptake, and enable targeted and controlled drug bio-delivery via surface modifications (Farahani et al. 2021). The ongoing developments in the nanomaterial antitumor strategies based on metal ions are yielding exciting and emerging impacts. For now, they are giving rise

to non-pharmaceutical theranostic agents wherein the metal ions that are integrated into the nanomaterial's building block, substitute for the traditional medicines (Liu et al. 2023). In particular, magnetic nanoparticles (MNPs) are largely used for biomedical applications due to their exceptional magnetic features, compatibility with living systems, and lack of toxicity. In this line, a considerable portion of the research is focused on designing multifunctional theranostic MNPs due to their ability to precisely target the affected organs, enabling direct monitoring of the therapy effectiveness through imaging techniques (Freis et al. 2023; Chu et al. 2013).

Magnetite ($\text{Fe(II)Fe(III)}_2\text{O}_4$) NPs, the well-known superparamagnetic compound, display remarkable genotoxic and cytotoxic characteristics. In addition to cell necrosis, mitochondrial disruption, DNA fragmentation, and changes in the expression of oncogenes, Fe_3O_4 NPs can lead to oxidative stress upon yielding reactive oxygen species (ROS), which causes cell apoptosis (Yew et al. 2020). Likewise, ceria (CeO_2) NPs are among the most potent agents for dealing with ROS-associated maladies, e.g., cancer. As per reports, cell proliferation can be promoted by Ce-incorporated mesoporous NPs without compromising the bioactivity (Tsamesidis et al. 2021). This is especially attributed to the existence of Ce^{3+} and Ce^{4+} in ceria, which can get switched between +3 and +4 upon pH alteration. Basically, when ceria NPs encounter tumor cells with an acidic pH, the oxidation state can be changed from +3 to +4, resulting in ROS production and thereupon, apoptosis is induced. However, the oxidation state can be converted from +4 to +3 under the neutral pH of the normal cells and assist the ROS elimination (Nourmohammadi et al. 2019).

Concerning the physical and chemical approaches for the synthesis of NPs, on the one hand, it typically applies high temperatures and pressures along with some type of radiation, on the other hand, employs toxic precursors which can pose risks and drive-up costs (Chormey et al. 2023). As a solution, the extracts and biological entities derived from various plants, algae, and fungi have been employed to biosynthesize various metallic NPs (Karunakaran et al. 2023). This method relies on the availability and abundance of plants and offers a safe, quick, and cost-effective alternative. The role of phytochemicals is especially significant in the synthesis of metal oxide NPs where they serve as reducing, capping, and/or stabilizing agents (Bayrami et al. 2019).

Sweet wormwood (*Artemisia annua* L.) has a long history of being used as a medicinal plant in Asia and Africa to treat malaria. This plant belongs to the Asteraceae family and its therapeutic properties are attributed to its large number of biologically active substances (Lang et al. 2019). The well-known medicinal compound of *A. annua* is artemisinin, which is a sesquiterpene lactone produced in the plant's trichomes (Fig. S1) (Krishna et al. 2008). Artemisinin possesses a crucial endoperoxide bridge that is essential for its bioactive properties (O'Neill and Posner 2004). The studies indicate that the anticancer potential of *A. annua* is not solely attributed to a single active phytochemical, e.g., artemisinin but more to its entire collection of phytochemicals, which includes over 600 compounds, primarily coumarins, sesquiterpenoids, enzymes, flavonoids, and steroids (Dilshad et al. 2020; Shinyuy et al. 2023; Firestone and Sundar 2009; Isani et al. 2019). Since, there was a notable absence of research investigating the combined anticancer effects of *A. annua* with functional metal oxides such as Fe_3O_4 and CeO_2 , the present research investigated their synergistic potential for cancer treatment. This research

addresses a critical gap in the literature and has the potential to advance both scientific understanding and clinical practice.

This study aimed to systematically investigate the therapeutic properties of Fe₂O₄/CeO₂ nanocomposite prepared in the presence of *A. annua* extract on breast cancer and compare it with the Fe₂O₄/CeO₂ nanocomposite without the action of *Artemisia annua*. At first, the prepared nanocomposites were characterized using XRD, TEM, SEM, DRS, FT-IR, and zeta potential analyses to explore their morphological, size, surface, structural, and optical features. Later, the orthotopic transplanted mouse models containing 4T1 breast cancer cells were used to assess the synergistic effects of combined Fe₃O₄ and CeO₂ nanocomposite without (FC) and with *A. annua* extract (AFC) on the prevention and treatment of breast cancer in vitro and in vivo. Finally, the cytotoxicity of the AFC sample on the healthy mice was examined and antineoplastic efficiencies of the green-synthesized sample were assessed in relation to untreated mice.

Methods

Plant extract preparation

The dried *A. annua* plant was acquired from a local supplier in the Ardabil, Northwestern Iran, and the authenticity was confirmed by a botanist. The *A. annua* plant was carefully cleaned using deionized water to eliminate any dust and impurities. Subsequently, it was air-dried at room temperature for a period of 72 h and then ground into a fine powder. After this, 50 g of the resulting powder was blended with a 70% ethanol solution and agitated on a rotary shaker for 72 h. The resulting extract was then filtered using filter paper and preserved in a dark environment at 4 °C.

Green synthesis of Fe₃O₄/CeO₂

The environmentally friendly Fe₂O₄/CeO₂ green nanocomposite with an equal 1:1 ratio was prepared via a co-precipitation method (Hassandoost et al. 2019; Rahim Pouran et al. 2020). In detail, the mixture of CeO₂ (1 g) and extract (20 mL) was introduced into a solution containing FeCl₃·6H₂O and FeCl₂·4H₂O. After stirring for 30 min under vacuum, the solution was subjected to reflux at 100 °C for 1 h. Subsequently, the resulting precipitate was separated and placed in an oven to dry for 24 h.

Physical–chemical characterization

The X-ray crystallography (XRD) patterns were obtained using an X-ray diffractometer apparatus (X'Pert Pro, Panalytical, Netherlands) with a scanning rate of 0.04°/s in the 2θ = 10°–80° Cu Kα radiation (k = 0.15406 nm), to verify the crystalline state of the samples. The Perkin Elmer Spectrum was employed to record FT-IR spectra in the range of 400–4000 cm⁻¹ to determine the interaction between the phytochemicals and the metallic compound. UV–Vis DRS spectra were recorded by Scinco 4100 (Scinco, Korea) UV-vis spectrophotometer from 300 to 800 nm using BaSO₄ for baseline correction. Energy-dispersive X-ray spectroscopy (EDX) analysis was used for chemical analysis of the samples employing (TESCAN MIRA2, TESCAN, Czech Republic) detector. The transmission electron microscopy (TEM) micrographs were collected by HF3300 (Hitachi, Japan) to check the microscale morphology, size, and chemical composition of the samples. Data on the surface morphology, crystallinity, and elemental composition

were obtained via SEM images (LEO 1430 VP, England). Zeta potential analysis (Malvern Instruments, Westborough, USA) was used to measure the electrical charge of the nanoparticles.

In vitro apoptosis assay

Cell culture

The 4T1 mouse breast cancer cell line was sourced from the Pasteur Institute, Iran, and maintained in Dulbecco's Modified Eagle Medium (DMEM) together with heat-inactivated fetal bovine serum (FBS, 10%) and 100 IU/mL of penicillin in a humidified incubator with 5% CO₂ at 37 °C.

Cell toxicity and viability assay (MTT assay)

To assess cell proliferation, 3-(4,5-dimethylthiazol-2-yl)-2,5-diphenyltetrazolium bromide (MTT) or tetrazolium salt was used as the MTT assay. The assay was conducted using cells from passages 2 to 4. In brief, the 4T1 cells in active growth were trypsinized, collected using 0.25% trypsin–EDTA, and seeded in 96-well plates at a density of 10,000 cells per well. After a 24-h incubation, the cells were treated with varying concentrations of the samples (100, 250, 500, 750, 1000 µg/mL) in separate wells for each concentration. The cells were then further incubated in a 5% CO₂ incubator for 24 h at 37 °C. The cell viability was determined via MTT (5 mg/mL) addition to each well and incubating for an additional 3–4 h at 37 °C. Then, dimethyl sulfoxide (DMSO, 100 µL) was used to dissolve the resulting formazan crystals, and the corresponding absorbance was recorded at 570 nm employing a spectrophotometer (Spectramax M5, Molecular Devices, Sunnyvale, CA, USA). Subsequently, the half-maximum inhibitory concentration (IC₅₀) value was set for the 4T1 cells. It is significant to highlight that the preliminary testing of lower concentrations (below 100 µg/mL) revealed minimal cytotoxicity, with the 100 µg/mL concentration showing approximately 97% and 74% cell viability, indicating low toxicity of the nanocomposites at lower doses. Therefore, higher concentrations were used to assess the dose-dependent cytotoxic effects more clearly.

Flow cytometry (FCM)

Flow cytometry (FCM) remains the preferred method for investigating the apoptotic process concerning cell type, triggering mechanisms, and timing. To assess apoptosis, Annexin V-FITC was utilized as an indicator of phosphatidylserine exposure, and propidium iodide (PI) was employed to mark dead cells, using the APOAF Annexin V-FITC apoptosis detection kit from Sigma-Aldrich.

In vivo apoptosis assay

Animal

We procured nine four-week-old adult BALB/c female mice from the animal facility at the University of Tehran, Faculty of Medicine and Health Sciences. Throughout the experiments, the guidelines outlined in the National Institute of Health's (NIH) care and use manual for laboratory animals (No. 8023, revised 1978) were adhered to and duly authorized by the Ardabil Animal Care and Use Committee (IR.UMA.REC.1400.030). These mice were allowed to adapt to the laboratory conditions, maintained at a

temperature of 24 ± 1 °C, and subjected to a 12-h dark–light cycle for a period of seven days before initiating the experiments.

Tumor induction

PBS (200 μ L) was combined with the 4T1 cells (2×10^6) and injected into the fourth inguinal mammary fat pads of 4-week-old female BALB/c mice. In this experiment, we had three groups: Group 1 ($n = 3$) consisted of healthy mice that underwent surgery to investigate any potential toxicity and inflammation caused by the nanocomposites. Group 2 ($n = 3$) comprised mice with induced breast tumors using 4T1 cells (2×10^6) and given PBS as the control. Group 3 ($n = 3$) included mice-induced breast tumors via 4T1 cells (2×10^6) and served as the treatment group. Both Groups 1 and 3 received 5 mg/kg of green-synthesized nanocomposites by intraperitoneal injection for two weeks (Lu et al. 2014). Throughout the study, the animals were closely monitored twice a day (morning and afternoon) for signs of clinical abnormalities, including toxicity, inflammation, changes in body weight, and food consumption. The individual body weights of all test animals were recorded before dosing on days 0, 1, 7, and 14. Calipers were used for the measurement of tumors and the volume of tumors was calculated via the formula: $V = 1/2$ (width² \times length) (Traynor et al. 2023).

Histopathology

When the tumors of the studied mice reached a size of 500–700 mm³, they were euthanized by CO₂ inhalation in accordance with ethical guidelines. The collected breast tumor samples were sectioned into 0.5 cm² pieces and preserved in 10% formalin for at least 48 h. Slides were prepared from these samples and stained with Harris hematoxylin and eosin (H&E) followed by examination under a Nikon light microscope (Tokyo, Japan) (Hölscher et al. 2023).

Statistical analysis

The experimental data were compared using two-way ANOVA and expressed as mean \pm SE. The differences were considered significant at $p < 0.05$. All statistical analyses were conducted using SPSS software (version 20).

Results and discussion

Characterization of materials

Figure 1a displays the XRD patterns of the synthesized Fe₃O₄/CeO₂ (FC) and *A. annua* extract-mediated Fe₃O₄/CeO₂ (AFC). For FC sample, the distinct diffraction peaks of Fe₃O₄ crystal are observed at 2 θ values of 18.75°, 30.52°, 35.72°, 37.82°, 43.57°, 54.47°, 57.72°, 63.32°, 66.42°, 72.17°, and 74.92°. These peaks correspond to the (111), (220), (311), (222), (400), (422), (511), (440), (300), (620), and (533) lattice planes of cubic Fe₃O₄ crystal (JCPDS No. 01-075-0449), respectively. In addition, the peaks at 2 θ values of 28.72°, 33.27°, 47.62°, 56.57°, 59.92°, 69.72°, 76.92°, and 79.47° attributed to the (111), (200), (220), (311), (222), (400), (331), and (420) planes signified the cubic fluorite lattice of cubic CeO₂ (JCPDS No. 00-034-0394) (Hassandoost et al. 2019). A similar pattern was observed for the AFC sample and the peaks indicating the magnetite and ceria crystals were identified in the corresponding pattern with a small shift towards smaller 2 θ values

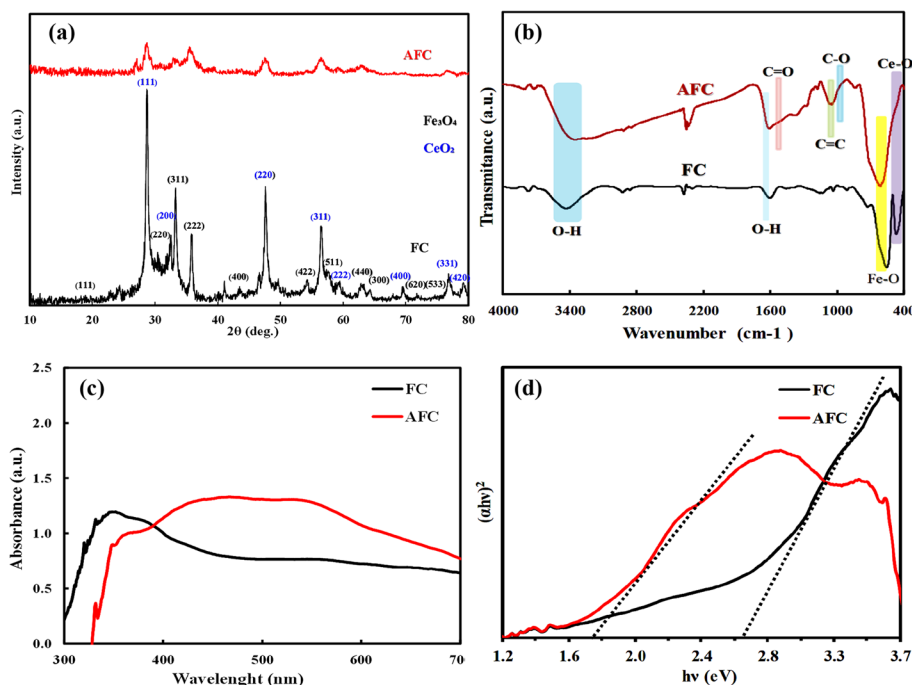


Fig. 1 a XRD patterns, b FT-IR spectra, c UV-Vis DRS spectra, and d band-gap values of FC and AFC samples

due to the presence of phytochemicals in the extract. Notably, in the case of the AFC, there is a significant reduction in the intensity of the peaks, indicating the presence of smaller particles (Franco et al. 2007). This suggests that the molecules from the *A. annua* extract have covered the surface of the $\text{Fe}_3\text{O}_4/\text{CeO}_2$ nanocomposites, resulting in a reduction in particle size (Rahim Pouran et al. 2020). As per the calculated crystallite sizes of the FC and AFC samples (15.58 nm and 7.14 nm) using XRD data in the Debye–Scherrer equation, the reduction in the crystallite sizes upon extract employment can be strongly verified.

FT-IR analysis was carried out to display the interaction of the phytochemicals of *A. annua* with Fe_3O_4 and CeO_2 via the identified functional groups on the surface of the samples (Fig. 1b). In the FC sample, the stretching vibration peaks of Fe–O and Ce–O bonds were detected at wavenumbers of 558 cm^{-1} and 464 cm^{-1} , respectively (Ventruti et al. 2016; Garcia et al. 2020). These peaks are observed as an overlapped intense peak at about 590 cm^{-1} with a shoulder at 472 cm^{-1} . Additional peaks related to the extract biomolecules were identified at 3756 cm^{-1} , 3376 cm^{-1} , 1608 cm^{-1} , 1372 cm^{-1} , and 1056 cm^{-1} , respectively, assigned to the O–H, N–H, C=C, phenolic O–H, and C–O bonds vibrations. The energy-dispersive X-ray spectroscopy (EDX) was parallel with FT-IR analysis (Fig. S2).

UV-vis diffuse reflectance spectroscopy (UV-vis DRS) was employed to examine the optical characteristics of both samples. As depicted in Fig. 1c, it is apparent that the level of light absorption in the visible region was notably higher for the extract-mediated sample when compared to $\text{Fe}_3\text{O}_4/\text{CeO}_2$ NC. As can be witnessed from the plotted Tauc (Fig. 1d), the band-gap energy of the AFC (1.78 eV) sample was significantly reduced compared to FC (2.62 eV), and its optical performance was greatly improved at the

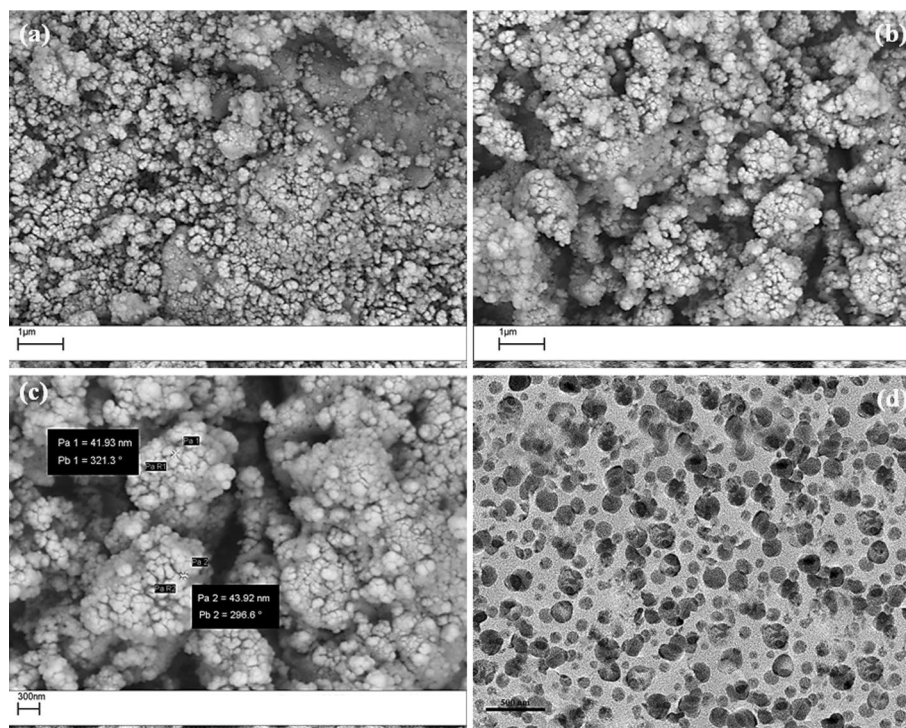


Fig. 2 SEM images of **a** FC and **b** AFC samples, **c** size and **d** TEM image of AFC sample

visible region, which can be mainly attributable to the large number of charge carriers from the extract phytochemicals (Khan et al. 2019).

Based on the characterization results, the *A. annua* extract appears to serve both as a reducing and capping agent in the synthesis of $\text{Fe}_3\text{O}_4/\text{CeO}_2$ nanocomposites. As per the UV–vis DRS analysis, the reduced band-gap energy and improved optical performance indicated that the extract could provide charge carriers, thus playing a reducing role. In addition to zeta potential results, FT-IR spectrum revealed the presence of functional groups from the extract, which are likely involved in stabilizing the nanoparticles, demonstrating its role as a capping agent (Rahim Pouran et al. 2020).

The SEM micrographs of FC and AFC samples exposed the clusters of spherical nanoparticles within the micrometer range (Fig. 2a–c). Due to the agglomeration of the particles, the observed average size for the AFC sample was around 42 nm in its SEM image. The TEM image of AFC displayed in Fig. 2d offers compelling evidence of the multitude of semi-spherical shapes and sizes. The TEM image further confirmed the particle size of AFC, and the provided scale bar indicated that the sizes were consistent with the XRD results, with smaller individual particles, though some aggregation was still apparent.

Zeta potential measurements were also carried out, yielding values of 29.7 mV for FC and -38.7 mV for AFC, as shown in Fig. S3. The zeta potential results indicated a significant difference in the surface charge properties of the two samples. The positive value of 29.7 mV for FC suggests a positively charged surface with good stability, as zeta potential values above $+30$ mV or below -30 mV typically indicate strong repulsive forces that help maintain dispersion stability. In contrast, the AFC sample has a zeta

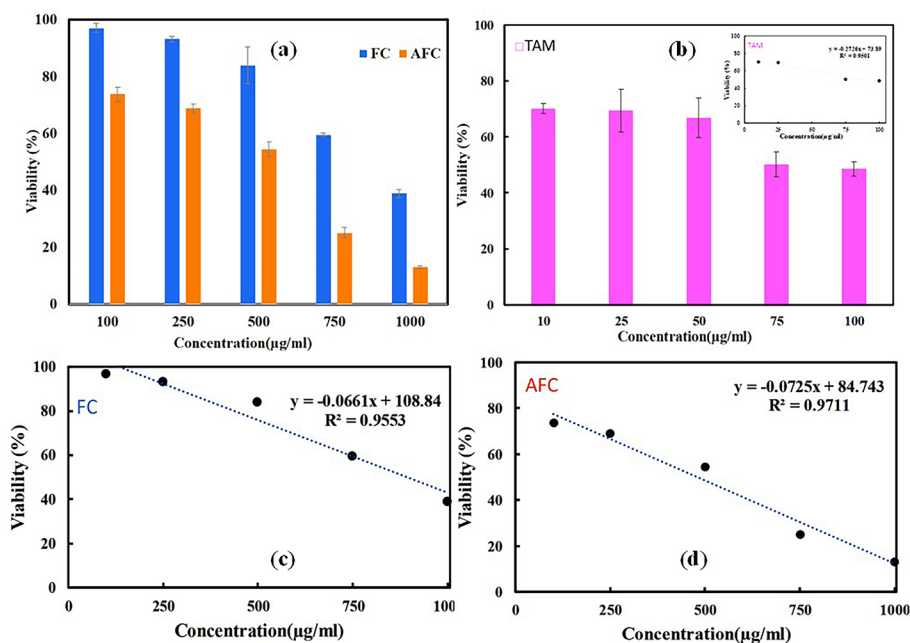


Fig. 3 **a** Cell viability of FC and AFC samples in comparison to one another and **b** tamoxifen; and IC_{50} values of FC and **d** AFC at varying concentrations [data are expressed as mean \pm standard error of the mean ($p < 0.05$)]

potential of -38.7 mV, indicating a highly negatively charged surface. This more negative value implies that the nanoparticles in AFC are even more stable in suspension due to the increased electrostatic repulsion between particles, which minimizes aggregation. The negative charge of AFC is likely attributed to the presence of anionic groups from the *A. annua* extract, enhancing the overall stability of the nanocomposite.

As per the characterizing analysis, the phytomolecules in the extract played a capping role by stabilizing smaller nanoparticles (as per XRD results) and a reducing role by providing charge carriers that facilitated the reduction of metal ions, as evidenced by the increased light absorption in the visible region.

Anticancer activity

Studies on cell viability and cytotoxicity

The cell viability was examined using the MTT assay to test the cytotoxicity of FC and AFC samples on 4T1 cells. For this purpose, the growth inhibition percentage of 4T1 cells was compared to the untreated cells when exposed to varying doses of the samples (100, 250, 500, 750, and 1000 $\mu\text{g}/\text{mL}$). Figure 3a illustrates the concentration-dependent growth inhibition of 4T1 cells. As per the results, the increase in the nanocomposite concentration enhanced the cytotoxic efficacies in both FC and AFC. In order to calculate the half-maximal inhibitory concentrations (IC_{50}) values of the samples, the fitted line obtained from the plotted dose–responses data was used to estimate the concentration at which the cell viability reached 50% (Iqbal et al. 2022). The IC_{50} values of 890.16 ($\mu\text{g}/\text{mL}$) and 490.21 ($\mu\text{g}/\text{mL}$) were determined within 24 h for FC and AFC, respectively. This not only indicates the time- and dose-dependency of the cytotoxic effects of the samples but also the higher effectiveness

of AFC to FC against 4T1 cells ($p < 0.05$). Data on the effectiveness of the well-known therapy, tamoxifen (TAM), were also collected and provided for comparison purposes ($IC_{50} = 87.63 \mu\text{g/mL}$). It is significant to highlight that the preliminary testing of lower concentrations (below $100 \mu\text{g/mL}$) revealed minimal cytotoxicity, with the $100 \mu\text{g/mL}$ concentration showing $\sim 97\%$ and 74% cell viability for FC and AFC nanocomposites, indicating their low toxicity at lower doses. Therefore, higher concentrations were used to assess the dose-dependent cytotoxic effects more clearly. This finding was in line with similar studies using lower concentrations of Fe_3O_4 and CeO_2 (Ebadi et al. 2020; Marzi et al. 2013).

Flow cytometry (FCM)

The apoptosis caused by *A. annua* plant extract synthesized $\text{Fe}_3\text{O}_4/\text{CeO}_2$ NC was further authenticated using Annexin V/propidium iodide (PI) assay for flow cytometry (Srichana et al. 2023). Figure 4 represents the flow cytometry profiles of the 4T1 cells' cycle phase distribution. As expected, significant apoptosis took place in the 4T1 cells upon exposure to AFC for about 24 h (Fig. 4). The AFC-treated 4T1 cells showed early and late apoptosis with death rates of 85.2% and 6.35% , respectively. In contrast, no significant apoptosis was observed in the untreated cells.

In vivo anticancer activity

Tumor size and body weight of BALB/c mouse models

More analyses were conducted to investigate whether the green-synthesized sample could effectively target the growth of the breast cancer cells in a living system where 4T1 cells-utilized BALB/c mice were employed as a xenograft model. Throughout the study, the healthy mice treated with AFC (via intraperitoneal injections at a dose of 5 mg/kg and for a duration of 2 weeks) did not exhibit any fatalities or signs of toxicity (Fig. 5). On the other hand, in the context of the antitumor investigation, the tumor size in mice treated with AFC was notably smaller than the untreated mice following the 2-week treatment period ($p < 0.05$, Fig. 5). The results strongly disclosed that the administration of AFC did not result in any discernible toxicity, as evidenced by the unchanged body weight of the studied mice.

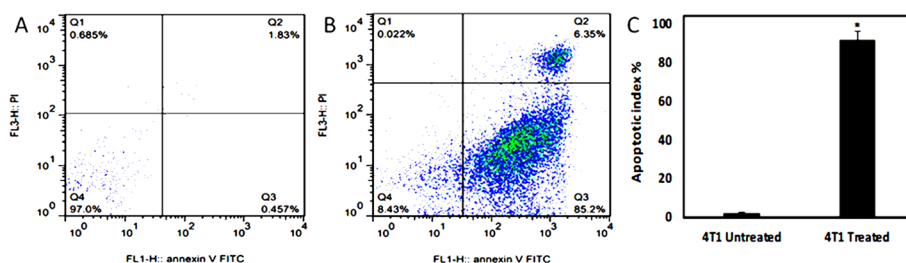


Fig. 4 a Flow cytometry analysis, b quadrangular plots representing the Annexin-V/PI expression in 4T1 cells upon exposure to c AFC (treated) and in the absence of AFC (untreated) ($p < 0.05$)

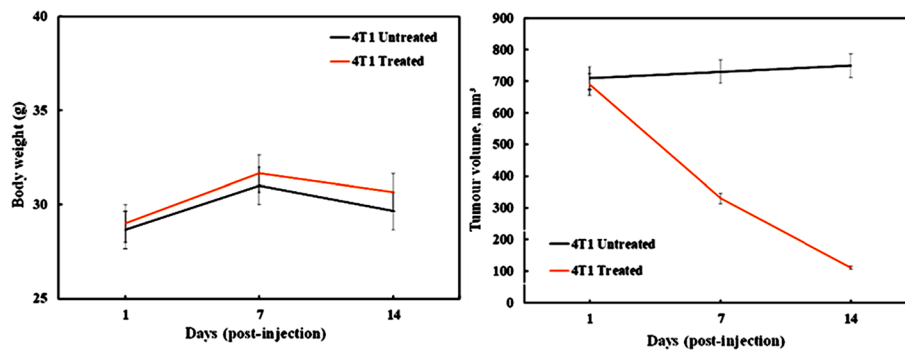


Fig. 5 The body weights and tumor sites of the AFC-treated and untreated mice (data are presented as mean \pm SD ($n=3$), (mm^3) ($*p < 0.05$))

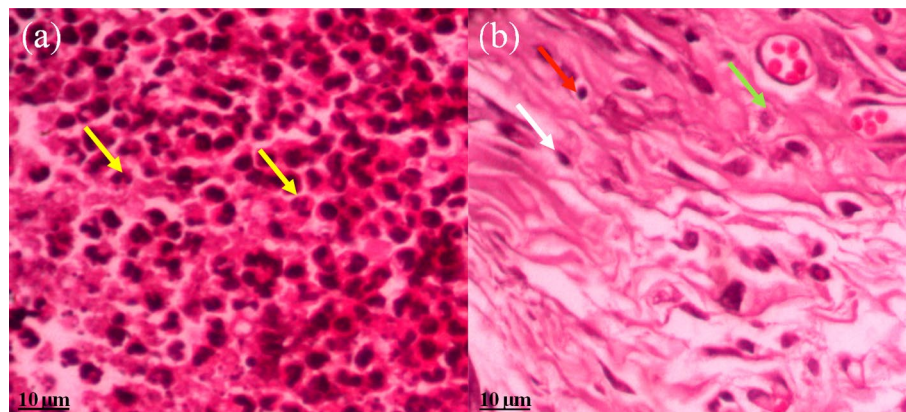


Fig. 6 Hematoxylin and eosin (H&E) staining of breast tumors (magnification: 100 \times): **a** untreated tumors, **b** AFC-treated tumors; apoptotic cells (red arrow), cellular debris (green arrow), and nuclear dust (white arrow)

Histopathology analysis

To compare the histopathological alterations in the tumors of untreated 4T1-injected mice with those of mice treated with AFC, breast tissues were collected, fixed, and subjected to hematoxylin and eosin (H&E) staining. Upon closer examination, higher magnification images of the untreated 4T1-injected mice breast tumors predominantly displayed viable tumor cells, characterized by pleomorphic vesicular nuclei and prominently hyperchromatic nucleoli (Fig. 6a). In contrast, higher magnification images of the AFC-treated 4T1 breast tumors revealed extensive areas of necrosis and late apoptosis, evident through the increased presence of apoptotic cells, cellular debris, and nuclear fragments (Fig. 6b).

The significant antineoplastic activity of *A. annua*-mediated $\text{Fe}_3\text{O}_4/\text{CeO}_2$ nanocomposite on 4T1 breast cancer cells can be explained as follows: Fe_3O_4 nanoparticles are capable of producing localized heating due to their magnetic property. This temperature rise can selectively destroy cancer cells, as they are more susceptible to heat than normal cells (Malehmir et al. 2023). Beyond this, magnetite can facilitate the generation of ROSs, which triggers oxidative stress in cancer cells and ultimately induces apoptosis (Paunovic et al. 2020). It is worth noting that the magnetic properties of Fe_3O_4 nanoparticles make them ideal candidates for drug delivery systems, enabling

the controlled release of drugs directly to tumor sites with the help of an external magnetic field, thereby limiting damage to healthy tissue (Blazkova et al. 2013). CeO₂ nanoparticles, on the other hand, possess the unique ability to shift between Ce³⁺ and Ce⁴⁺ oxidation states. This property allows them to neutralize excessive ROS in healthy cells while simultaneously promoting ROS production in cancer cells, thereby causing oxidative stress and triggering cell death through apoptosis. This selective ROS regulation is central to the anticancer activity of ceria (Selvaraj et al. 2024). Furthermore, CeO₂ nanoparticles can imitate the behavior of certain enzymes, such as superoxide dismutase and catalase, disrupting the redox balance in cancer cells and leading to their death through oxidative stress (Tang et al. 2023). Upon the combination of Fe₃O₄ and CeO₂, their ability to regulate oxidative stress is amplified, creating a synergistic effect. This combined action enhanced their therapeutic potential and resulted in increased cancer cell apoptosis and overall efficacy in cancer treatment.

Moreover, as per the findings of the in vivo and in vitro studies, it can be strongly deduced that the extract phytomolecules have a prominent role in enhancing the anti-proliferative efficacy of the studied nanocomposite. The extract of *A. annua* significantly boosts the anticancer effectiveness of nanocomposites, attributed to its abundant bioactive phytomolecules (Lang et al. 2019). These compounds can trigger apoptosis in cancer cells by elevating oxidative stress and interfering with cell cycle progression (Cao et al. 2019). Several studies have reported the antitumor action of artemisinin and its derivatives as one of the frequently studied secondary metabolites of *A. annua* due to its preventive effects on inflammation and cell damage resulting from necrosis (Crespo-Ortiz and Wei 2012; Slezakova and Ruda-Kucerova 2017). Moreover, the green route of synthesizing nanostructures supplies a safe and biocompatible approach to preparing therapeutically active alternatives. The extract functions as a reducing agent during the synthesis of nanoparticles, enhancing their stability. Its phytomolecules also act as capping agents, which not only improve biocompatibility, but also promote the selective targeting of tumor tissues (Villagrán et al. 2024). This dual function of *A. annua* extract, as both a therapeutic agent and a stabilizing component, highlights its critical role in the as-prepared nanocomposite for effective breast cancer treatment.

Conclusion

In this study, we successfully synthesized Fe₃O₄/CeO₂ magnetic nanocomposites using both chemical (FC) and *A. annua* extract (AFC). FT-IR and EDX analyses confirmed the presence of Fe₃O₄ and CeO₂ in both samples, while AFC also incorporated phytomolecules from the extract. AFC demonstrated smaller particle size (7.14 nm) compared to FC (15.58 nm), more uniform morphology, and enhanced optical properties (band-gap energy reduced to 1.78 eV compared to 2.62 eV for FC), which can be attributed to the dual capping and reducing effects of the *A. annua* extract. The in vitro cytotoxicity assays on 4T1 breast cancer cells demonstrated the superior anticancer efficacy of AFC over FC, with IC₅₀ values of 490.21 µg/mL for AFC and 890.16 µg/mL for FC. On the other hand, the flow cytometry analysis showed that AFC induced substantial apoptosis in 4T1 cells after 24 h of exposure, supporting its enhanced cytotoxicity. The significant roles of the extract at the nanoscale level contributed to these cellular responses by modulating the surface properties and bioactivity of the nanocomposite. The in vivo

studies exhibited no signs of toxicity or fatalities in the AFC-treated healthy mice, while tumor size in AFC-treated mice significantly decreased compared to the untreated control group. Histopathological analysis confirmed notable antineoplastic effects in AFC-treated mice, characterized by an increased number of apoptotic cells, cellular debris, and nuclear fragments in breast tissue samples. This further highlighted the efficacy of AFC in selectively targeting cancer cells without causing harm to healthy tissues. It should be underlined that the dual capping and reducing roles of *A. annua* extract, along with its anticancer phytochemicals, enhanced both the nanocomposite properties and the therapeutic efficacy of AFC against cancer cells. The combined anticancer effects of Fe_3O_4 , CeO_2 , and the *A. annua* extract emphasize their potential as a synergistic therapeutic strategy in breast cancer treatment. Future studies are encouraged to explore its application in combination therapies and investigate its underlying mechanisms of action.

Supplementary Information

The online version contains supplementary material available at <https://doi.org/10.1186/s12645-024-00294-y>.

Supplementary Material 1.

Acknowledgements

The authors are grateful for the support provided by the University of Mohaghegh Ardabili.

Author contributions

Ziba Ahmadi (Z.A) Abolfazl Bayrami (A.B) Saber Zahri (S.Z) Shima Rahim Pouran (S.RP) Aziz Habibi-Yangjeh (A.HY) Z.A Did the experimental work. A.B and S.Z were supervisors. S.RP and A.HY were the project advisors. All authors except Z.A completed the methodology. Z.A and S.RP wrote the main manuscript text. All authors except Z.A reviewed the manuscript. A.B, S.Z, and A.HY provided resources.

Funding

This research received no specific grant from any funding agency in the public, commercial, or not-for-profit sectors.

Availability of data and materials

No datasets were generated or analysed during the current study.

Declarations

Ethics approval and consent to participate

The guidelines outlined in the National Institute of Health's (NIH) care and use manual for laboratory animals (No. 8023, revised 1978) were adhered to throughout the experiments and duly authorized by the Ardabil Animal Care and Use Committee (IR.UMA.REC.1400.030).

Consent for publication

Not applicable.

Competing interests

The authors declare no competing interests.

Received: 29 June 2024 Accepted: 27 September 2024

Published online: 19 October 2024

References

- Arnold M, Morgan E, Rumgay H, Mafra A, Singh D, Laversanne M, Vignat J, Gralow JR, Cardoso F, Siesling S et al (2022) Current and future burden of breast cancer: global statistics for 2020 and 2040. *The Breast* 66:15–23
- Bayrami A, Alioghli S, Rahim Pouran S, Habibi-Yangjeh A, Khataee A, Ramesh S (2019) A facile ultrasonic-aided biosynthesis of ZnO nanoparticles using *Vaccinium arctostaphylos* L. leaf extract and its antidiabetic, antibacterial, and oxidative activity evaluation. *Ultrasonics Sonochem* 55:57–66
- Beňačka R, Szabóová D, Guľašová Z, Hertelyová Z, Radoňák J (2022) Classic and new markers in diagnostics and classification of breast cancer. *Cancers* 14(21):5444

- Blazkova I, Nguyen HV, Dostalova S, Kopel P, Stanisavljevic M, Vaculovicova M, Stiborova M, Eckschlager T, Kizek R, Adam V (2013) Apoferritin modified magnetic particles as doxorubicin carriers for anticancer drug delivery. *Int J Mol Sci* 14(7):13391–13402
- Brandão SR, Reis-Mendes A, Duarte-Araújo M, Neuparth MJ, Rocha H, Carvalho F, Ferreira R, Costa VM (2023) Cardiac molecular remodeling by anticancer drugs: doxorubicin affects more metabolism while mitoxantrone impacts more autophagy in adult CD-1 male mice. *Biomolecules* 13(6):921
- Brown T, Sykes D, Allen AR (2021) Implications of breast cancer chemotherapy-induced inflammation on the gut, liver, and central nervous system. *Biomedicines* 9(2):189
- Cao Y, Feng Y-H, Gao L-W, Li X-Y, Jin Q-X, Wang Y-Y, Xu Y-Y, Jin F, Lu S-L, Wei M-J (2019) Artemisinin enhances the anti-tumor immune response in 4T1 breast cancer cells in vitro and in vivo. *Int Immunopharmacol* 70:110–116
- Chormey DS, Zaman BT, Borahan Kustanto T, Erarpat Bodur S, Bodur S, Tekin Z, Nejati O, Bakirdere S (2023) Biogenic synthesis of novel nanomaterials and their applications. *Nanoscale* 15(48):19423–19447
- Chu M, Shao Y, Peng J, Dai X, Li H, Wu Q, Shi D (2013) Near-infrared laser light mediated cancer therapy by photothermal effect of Fe₃O₄ magnetic nanoparticles. *Biomaterials* 34(16):4078–4088
- Crespo-Ortiz MP, Wei MQ (2012) Antitumor activity of artemisinin and its derivatives: from a well-known antimalarial agent to a potential anticancer drug. *J Biomed Biotechnol* 2012:247597
- Davezac M, Meneur C, Buscato M, Zahreddine R, Arnal J-F, Dalenc F, Lenfant F, Fontaine C (2023) The beneficial effects of tamoxifen on arteries: a key player for cardiovascular health of breast cancer patient. *Biochem Pharmacol* 214:115677
- De Marzi L, Monaco A, De Lapuente J, Ramos D, Borrás M, Di Gioacchino M, Santucci S, Poma A (2013) Cytotoxicity and genotoxicity of ceria nanoparticles on different cell lines in vitro. *Int J Mol Sci* 14(2):3065–3077
- Dilshad E, Ismail H, Khan MA, Cusido RM, Mirza B (2020) Metabolite profiling of *Artemisia carvifolia* Buch transgenic plants and estimation of their anticancer and antidiabetic potential. *Biocatal Agric Biotechnol* 24:101539
- Dy GK, Adjei AA (2013) Understanding, recognizing, and managing toxicities of targeted anticancer therapies. *CA Cancer J Clin* 63(4):249–279
- Ebadi M, Buskaran K, Bullo S, Hussein MZ, Fakurazi S, Pastorin G (2020) Synthesis and cytotoxicity study of magnetite nanoparticles coated with polyethylene glycol and sorafenib-zinc/aluminium layered double hydroxide. *Polymers (Basel)* 12(11):2716
- Farahani M, Moradikhah F, Shabani I, Soflou RK, Seyedjafari E (2021) Microfluidic fabrication of berberine-loaded nanoparticles for cancer treatment applications. *J Drug Deliv Sci Technol* 61:102134
- Ferlay J, Colombet M, Soerjomataram I, Parkin DM, Piñeros M, Znaor A, Bray F (2021) Cancer statistics for the year 2020: an overview. *Int J Cancer* 149:778–789
- Firestone GL, Sundar SN (2009) Anticancer activities of artemisinin and its bioactive derivatives. *Expert Rev Mol Med* 11:e32
- Franco F, Cecilia JA, Pérez-Maqueda LA, Pérez-Rodríguez JL, Gomes CSF (2007) Particle-size reduction of dickite by ultrasound treatments: effect on the structure, shape and particle-size distribution. *Appl Clay Sci* 35(1):119–127
- Freis B, Ramirez MDLA, Kiefer C, Harlepp S, Iacovita C, Henoumont C, Affolter-Zbarszczuk C, Meyer F, Mertz D, Boos A et al (2023) Effect of the size and shape of dendronized iron oxide nanoparticles bearing a targeting ligand on MRI, magnetic hyperthermia, and photothermia properties from suspension to in vitro studies. *Pharmaceutics* 15(4):1104
- Garcia IM, Leitune VCB, Takimi AS, Bergmann CP, Samuel SMW, Melo MA, Collares FM (2020) Cerium dioxide particles to tune radiopacity of dental adhesives: microstructural and physico-chemical evaluation. *J Funct Biomater* 11(1):7
- Hassandoost R, Pouran SR, Khataee A, Orooji Y, Joo SW (2019) Hierarchically structured ternary heterojunctions based on Ce³⁺/Ce⁴⁺ modified Fe₃O₄ nanoparticles anchored onto graphene oxide sheets as magnetic visible-light-active photocatalysts for decontamination of oxytetracycline. *J Hazard Mater* 376:200–211
- Hölscher DL, Bouteldja N, Joodaki M, Russo ML, Lan Y-C, Sadr AV, Cheng M, Tesar V, Stillfried SV, Klinkhammer BM et al (2023) Next-generation morphometry for pathomics-data mining in histopathology. *Nat Commun* 14(1):470
- Iqbal H, Razaq A, Khan NU, Rehman SU, Webster TJ, Xiao R, Menaa F (2022) pH-responsive albumin-coated biopolymeric nanoparticles with lapatinib for targeted breast cancer therapy. *Biomater Adv* 139:213039
- Isani G, Bertocchi M, Andreani G, Farruggia G, Cappadone C, Salaroli R, Forni M, Bernardini C (2019) Cytotoxic effects of *Artemisia annua* L. and pure artemisinin on the D-17 canine osteosarcoma cell line. *Oxid Med Cell Longev* 2019:1615758
- Jin C, Wang K, Oppong-Gyebi A, Hu J (2020) Application of nanotechnology in cancer diagnosis and therapy—a mini-review. *Int J Med Sci* 17(18):2964
- Karunakaran G, Sudha KG, Ali S, Cho EB (2023) Biosynthesis of nanoparticles from various biological sources and its biomedical applications. *Molecules* 28(11):4527
- Khan MM, Saadah NH, Khan ME, Harunsani MH, Tan AL, Cho MH (2019) Potentials of *Costus woodsonii* leaf extract in producing narrow band gap ZnO nanoparticles. *Mater Sci Semicond Process* 91:194–200
- Krishna S, Bustamante L, Haynes RK, Staines HM (2008) Artemisinins: their growing importance in medicine. *Trends Pharmacol Sci* 29(10):520–527
- Lang SJ, Schmiech M, Hafner S, Paetz C, Steinborn C, Huber R, Gaafary ME, Werner K, Schmidt CQ, Syrovets T et al (2019) Antitumor activity of an *Artemisia annua* herbal preparation and identification of active ingredients. *Phytomedicine* 62:152962
- Liu C, Guo L, Wang Y, Zhang J, Fu C (2023) Delivering metal ions by nanomaterials: turning metal ions into drug-like cancer theranostic agents. *Coord Chem Rev* 494:215332
- Lu J, Zhao W, Huang Y, Liu H, Marquez R, Gibbs RB, Li J, Venkataraman R, Xu L, Li S et al (2014) Targeted delivery of Doxorubicin by folic acid-decorated dual functional nanocarrier. *Mol Pharm* 11(11):4164–4178
- Malehmir S, Esmaili MA, Khaksary Mahabady M, Sobhani-Nasab A, Atapour A, Ganjali MR, Ghasemi A, Moradi Hasan-Abad A (2023) A review: hemocompatibility of magnetic nanoparticles and their regenerative medicine, cancer therapy, drug delivery, and bioimaging applications. *Front Chem*. 11
- Manouchehri E, Taghipour A, Ebadi A, Homaei Shandiz F, Latifnejad Roudsari R (2022) Understanding breast cancer risk factors: is there any mismatch between laywomen perceptions and expert opinions. *BMC Cancer* 22(1):309

- Nourmohammadi E, Khoshdel-sarkarizi H, Nedaenia R, Sadeghnia HR, Hasanzadeh L, Darroudi M, Kazemi oskuee R (2019) Evaluation of anticancer effects of cerium oxide nanoparticles on mouse fibrosarcoma cell line. *J Cell Physiol* 234(4):4987–4996
- O'Neill PM, Posner GH (2004) A medicinal chemistry perspective on artemisinin and related endoperoxides. *J Med Chem* 47(12):2945–2964
- Paunovic J, Vucevic D, Radosavljevic T, Mandić-Rajčević S, Pantic I (2020) Iron-based nanoparticles and their potential toxicity: focus on oxidative stress and apoptosis. *Chem Biol Interact* 316:108935
- Pellegrini M, Merlo FD, Agnello E, Monge T, Devecchi A, Casalone V, Montemurro F, Ghigo E, Sapino A, Bo S (2023) Dysgeusia in patients with breast cancer treated with chemotherapy—a narrative review. *Nutrients* 15(1):226
- Rahim Pouran S, Bayrami A, Mohammadi Arvanag F, Habibi-Yangjeh A, Darvishi Cheshmeh Soltani R, Singh R, Abdul Raman AA, Chae KH, Khataee A, Kang HK (2020) Biogenic integrated ZnO/Ag nanocomposite: surface analysis and in vivo practices for the management of type 1 diabetes complications. *Colloids Surf B Biointerfaces* 189:110878
- Riggio AI, Varley KE, Welm AL (2021) The lingering mysteries of metastatic recurrence in breast cancer. *Br J Cancer* 124(1):13–26
- Selvaraj S, Chauhan A, Radhakrishnan A, Rana G, Dutta V, Batoo KM, Ghotakar S (2024) Cerium oxide nanoparticles and their polymeric composites: advancements in biomedical applications. *J Inorg Organometall Polym Mater*. <https://doi.org/10.1007/s10904-024-03263-5>
- Shinyuy LM, Loe GE, Jansen O, Mamede L, Ledoux A, Noukimi SF, Abenwie SN, Ghogomu SM, Souopgui J, Robert A et al (2023) Secondary metabolites isolated from *Artemisia afra* and *Artemisia annua* and their anti-malarial, anti-inflammatory and immunomodulating properties-pharmacokinetics and pharmacodynamics: a review. *Metabolites* 13(5):613
- Singh NK, Beckett JM, Kalpurath K, Ishaq M, Ahmad T, Eri RD (2023) Synbiotics as supplemental therapy for the alleviation of chemotherapy-associated symptoms in patients with solid tumours. *Nutrients* 15(7):1759
- Slezakova S, Ruda-Kucerova J (2017) Anticancer activity of artemisinin and its derivatives. *Anticancer Res* 37(11):5995–6003
- Srichana T, Thawithong E, Nakpheng T, Paul PK (2023) Flow cytometric analysis, confocal laser scanning microscopic, and holotomographic imaging demonstrate potentials of levofloxacin dry powder aerosols for TB treatment. *J Drug Deliv Sci Technol* 84:104464
- Tang JLY, Moonshi SS, Ta HT (2023) Nanoceria: an innovative strategy for cancer treatment. *Cell Mol Life Sci* 80(2):46
- Traynor S, Terp MG, Nielsen AY, Guldborg P, Jakobsen M, Pedersen PG, Gammelgaard OL, Pedersen CB, Pedersen MT, Rattenborg S et al (2023) DNA methyltransferase inhibition promotes recruitment of myeloid-derived suppressor cells to the tumor microenvironment through induction of tumor cell-intrinsic interleukin-1. *Cancer Lett* 552:215982
- Tsamesidis I, Gkiliopoulos D, Pouroutzidou GK, Lymperaki E, Papoulia C, Reybier K, Perio P, Paraskevopoulos KM, Kontonasaki E, Theocharidou A (2021) Effect of artemisinin-loaded mesoporous cerium-doped calcium silicate nanopowder on cell proliferation of human periodontal ligament fibroblasts. *Nanomaterials* 11(9):2189
- Ventruți G, Ventura GD, Bellatreccia F, Lacalamita M, Emanuela S (2016) Hydrogen bond system and vibrational spectroscopy of the iron sulfate fibroferrite, $\text{Fe}(\text{OH})\text{SO}_4 \cdot 5\text{H}_2\text{O}$. *Eur J Mineral* 28(5):943–952
- Villagrán Z, Anaya-Esparza LM, Velázquez-Carriles CA, Silva-Jara JM, Ruvalcaba-Gómez JM, Aurora-Vigo EF, Rodríguez-Lafitte E, Rodríguez-Barajas N, Balderas-León I, Martínez-Esquívias F (2024) Plant-based extracts as reducing, capping, and stabilizing agents for the green synthesis of inorganic nanoparticles. *Resources* 13(6):70
- Waks AG, Winer EP (2019) Breast cancer treatment: a review. *JAMA* 321(3):288–300
- Wang Y, Iqbal H, Ur-Rehman U, Zhai L, Yuan Z, Razzaq A, Lv M, Wei H, Ning X, Xin J et al (2023) Albumin-based nanodevices for breast cancer diagnosis and therapy. *J Drug Deliv Sci Technol* 79:104072
- Yew YP, Shamelı K, Miyake M, Ahmad Khairudin NBB, Mohamad SEB, Naiki T, Lee KX (2020) Green biosynthesis of superparamagnetic magnetite Fe_3O_4 nanoparticles and biomedical applications in targeted anticancer drug delivery system: a review. *Arab J Chem* 13(1):2287–2308
- Zajączkowska R, Kocot-Kępska M, Leppert W, Wrzosek A, Mika J, Wordliczek J (2019) Mechanisms of chemotherapy-induced peripheral neuropathy. *Int J Mol Sci* 20(6):1451

Publisher's Note

Springer Nature remains neutral with regard to jurisdictional claims in published maps and institutional affiliations.